Accepted manuscript of: A. Bekasiewicz, V. Waladi, M. Wojcikowski and T. -V. Cao, "Automatic Correction of Non-Anechoic Antenna Measurements using Low-Pass Filters," 2023 IEEE Conference on Antenna Measurements and Applications (CAMA), Genoa, Italy, 2023, pp. 786-789, doi: 10.1109/CAMA57522.2023.10352730.

Automatic Correction of Non-Anechoic Antenna Measurements using Low-Pass Filters

Adrian Bekasiewicz
Faculty of ETI
Gdansk University of Technology
Gdansk, Poland
bekasiewicz@ru.is

Vorya Waladi
Faculty of ETI
Gdansk University of Technology
Gdansk, Poland
vorya.waladi@pg.edu.pl

Marek Wojcikowski
Faculty of ETI
Gdansk University of Technology
Gdansk, Poland
marek.wojcikowski@pg.edu.pl

Tuan-Vu Cao
Dept. of Digital Tech.
Norwegian Institute for Air Research
Oslo, Norway
tvc@nilu.no

***Abstract*—Prototype measurements belong to key steps in the development of antenna structures. They are normally performed in expensive facilities, such as anechoic chambers (ACs). Alternatively, antenna performance can be extracted (at a low cost) in non-anechoic conditions upon appropriate post-processing. Unfortunately, existing correction algorithms are difficult to set up and prone to failure, which limits their practical usefulness. In this work, a method for refining far-field antenna responses that exploits a series of low-pass filters with automatically determined properties has been proposed. Its performance has been demonstrated using a geometrically small antipodal Vivaldi radiator measured in an office room. The approach has been favorably compared against the state-of-the-art techniques from the literature.**

Keywords—antennas, auto calibration, non-anechoic measurements, post-processing, radiation pattern.

I. Introduction

Measurements are inevitable for the validation of real-world antenna performance. Far-field responses of radiators are normally characterized in expensive facilities such as anechoic chambers (ACs), compact-range, or open-test sites [1]. Although capable of ensuring high (certification-grade) accuracy, professional facilities might be too expensive for training-oriented applications, or low-budget research [2]-[4]. Alternatively, antennas can be characterized in non-anechoic conditions, where—contrary to conventional laboratories—the control of the propagation environment is neglected [5]-[10]. However, due to multi-path interferences and noise from external sources of electromagnetic (EM) radiation, appropriate post-processing is required to draw meaningful conclusions on the real-world performance of antennas tested in such conditions [1], [8], [13].

Post-processing methods applicable to non-anechoic test sites fall into two main categories: (i) decomposition of the measured responses, and (ii) characterization of the propagation environment [5]-[14]. The first class of methods focuses on extracting the useful part of the S_{21} response—pertinent to the Line-of-Sight (LoS)—transmitted between the reference antenna (RA) and the antenna under test (AUT) [1]. The problem can be addressed using both frequency- and time-domain methods [5]-[11]. The former class of techniques involves approximation of the signal (based on multi- or single-point processing) using appropriately defined basis functions in the form of, e.g., Chebyshev polynomials, complex exponentials, or spherical-wave coefficients [9]-[11]. The generated approximation is then truncated to the set of components featuring the highest contribution to the overall response (determined, e.g., based on their amplitude), while neglecting the remaining ones [9]-[11]. Time-domain correction methods are oriented towards conversion of the frequency-based measurements using the inverse Fourier transform [5]-[8]. The resulting impulse response is then processed using an appropriately defined gating function and the modified signal is converted back to the frequency-domain for extraction of the far-field performance at the frequency of interest [5]-[8]. It is worth noting that the considered methods are to be executed separately at each RA-AUT angle of interest. The second class of techniques allows for the extraction of environmental effects on the AUT performance based on multiple experiments. In [15], a mechanism that involves three separate measurements of the structure in different locations of the same test site has been proposed. Upon data acquisition, the far-field antenna responses have been calculated based on a comparative analysis of the obtained signals. An approach oriented towards extraction of the noise floor followed by refinement of the corrupted AUT response using the obtained data has been presented in [7]. In [14], the correction process based on characterization of the probe antenna in perfect and non-ideal EM simulation environments has been considered. The difference between the responses in both conditions have been then used to refine AUT characteristics. Performance reconstruction based on analysis of the equivalent currents computed on a hull that encloses the antenna has also been considered [12].

Despite the demonstrated usefulness, post-processing methods from the literature are difficult to set up, and their performance heavily depends on adjustment of the control parameters [5], [6], [8], [15]. The latter ones are normally determined based on manual or semi-manual tuning, which is time-consuming and prone to failure. Another problem is that the state-of-the-art routines are predominantly validated in idealized conditions such as anechoic chambers with installed reflective surfaces, or EM-simulation environments [5], [6], [10], [14]. The former, due to strict control of the propagation environment, offer much less challenging conditions compared to, e.g., office rooms that are not tailored to far-field tests [8], [13]. Simulation-based setups, on the other hand, can be considered stationary in time—due to lack of random noise induced by the EM external sources—which simplifies analysis [14]. From this perspective, the problem concerning reliable, automatic correction of non-anechoic measurements for day-to-day use remains open.

In this work, a method for correcting far-field antenna responses obtained in uncontrolled propagation conditions has been proposed. The approach involves the automatic determination of the part of the signal that corresponds to LoS and non-LoS RA-AUT transmission. The identified response is then utilized to automatically synthesize prototypes of low-pass filters, which are further applied to correct noisy responses obtained at the non-anechoic test-site. The performance of the method has been validated through measurements of a geometrically small Vivaldi antenna in a standard office room (i.e., not tailored to far-field measurements). Validation against the state-of-the-art methods from the literature has also been provided.

II. Methodology

Let $\boldsymbol{R}(\boldsymbol{\omega}, \boldsymbol{\theta})$ denote a complex S_{21} transmission obtained in non-anechoic conditions between the reference antenna and the AUT, where $\boldsymbol{\omega} = [\omega_1 \ \ldots \ \omega_K]^T$ and $\boldsymbol{\theta} = [\theta_1 \ \ldots \ \theta_A]^T$ denote the K-point frequency sweep and angular positions of the AUT w.r.t. RA, respectively. Note that $B = \omega_K + \omega_1$ represents the bandwidth around the center frequency given as $f_0 = 0.5(\omega_K + \omega_1)$. The correction process implements a transformation h: $\boldsymbol{R} \rightarrow \boldsymbol{R}_c$, where $\boldsymbol{R}_c = \boldsymbol{R}_c(f_0, \boldsymbol{\theta})$ is the radiation pattern refined using the set of appropriately defined low-pass filters [16]. The post-processing is executed separately at each angle of rotation θ_a, $a = 1, \ldots, A$.

The first step of the algorithm involves determining the LoS-to-non-LoS delay. Let $\boldsymbol{P}(\boldsymbol{t}, \theta_a) = F^{-1}(\boldsymbol{R}(\boldsymbol{\omega}, \theta_a), N) \circ (F^{-1}(\boldsymbol{R}(\boldsymbol{\omega}, \theta_a), N))^H$ be the complex N-point power response of the RA-AUT system at the θ_a angle, where $F^{-1}(\cdot)$, "$\circ$", and "H" denote the inverse Fourier transform, component-wise multiplication, and Hermitian transpose, respectively. The time sweep is $\boldsymbol{t} = [t_1, \ldots, t_N]^T = \partial t \cdot \boldsymbol{M}$; $\partial t = B^{-1}$, $\boldsymbol{M} = [-N/2, \ldots, N/2-2, N/2-1]^T$, and $N = 2^{\lceil \log_2(K) \rceil + 3}$ (the symbol $\lceil \cdot \rceil$ represents rounding up to the nearest integer). The LoS profile is extracted as a result of the following process. First, the vector of delays $\boldsymbol{t}_d^{(j)} = [t_{d.1}^{(j)} \ \ldots \ t_{d.a}^{(j)} \ \ldots \ t_{d.A}^{(j)}]^T$ ($j = 1$) is extracted as:

$$t_a^{(j)} = \underset{\substack{t_a^{(j)} \in \boldsymbol{t} \\ t_l^{(j)} \le t_a^{(j)} \le t_h^{(j)}}}{\arg\max} \left(\boldsymbol{P}(\boldsymbol{t}, \theta_a) \right) \tag{1}$$

where $t_l^{(1)} = 0$ and $t_h^{(1)} = \partial t \cdot (N/2-1)$ represent boundaries for identification of the signal maxima (note that the power response is confined within $\boldsymbol{t}$). Having in mind that—due to challenging propagation conditions in non-anechoic test-sites—the contents of $\boldsymbol{t}_d^{(1)}$ might inaccurately represent the LoS delays as a function of angular position [13], the procedure (1) is repeated ($j = 2$) with the redefined bounds $t_l^{(2)} = t_{\text{opt}} - \alpha \cdot w_0$ and $t_h^{(2)} = t_{\text{opt}} + \alpha \cdot w_0$. The control parameters $t_{\text{opt}} = \min(\boldsymbol{t}_d^{(1)})$ and w_0 represent the shortest (implicitly corresponding to LoS) RA-AUT delay and half-prominence of the time-domain LoS power pulse (i.e., its width at half of its height) [17]; time-span scaling is set to $\alpha = 3$. The refined vector $\boldsymbol{t}_0 = [t_{0.1}^{(j)} \ \ldots \ t_{0.a}^{(j)} \ \ldots \ t_{0.A}^{(j)}]^T = \boldsymbol{t}_d^{(2)}$ is used as a reference for the determination of the delays pertinent to non-LoS interferences.

The LoS peaks of individual power responses $\boldsymbol{P}_a = \boldsymbol{P}(\boldsymbol{t}, \theta_a) = [P(t_1, \theta_a) \ P(t_2, \theta_a) \ \ldots \ P(t_{0.a}, \theta_a) \ \ldots \ P(t_N, \theta_a)]^T$ are aligned according to the $\boldsymbol{t}_0$ components such that $\boldsymbol{P}_s = [\boldsymbol{P}_{s.1} \ \ldots \ \boldsymbol{P}_{s.a} \ \ldots \ \boldsymbol{P}_{s.A}]^T$, where $\boldsymbol{P}_{s.a}$ represents the normalized vector of the following form: $\boldsymbol{P}_{s.a} = [P(t_{0.a}, \theta_a), \ldots, P(t_N, \theta_a), P(t_{0.1}, \theta_a), \ldots, P(t_{0.a-1}, \theta_a)]^T / \max(\boldsymbol{P}_a)$. Next, a response $\boldsymbol{P}_c = [P_{c.1} \ \ldots \ P_{c.q} \ \ldots \ P_{c.Q}]^T$ is calculated. Its qth element, $P_{c.q}$ corresponds to qth-row components averaged across all columns of the $\boldsymbol{P}_s$ vector (i.e., obtained w.r.t. all $\boldsymbol{\theta}$ angles). Note that $q = 1, \ldots, Q$, where Q ($Q < N$) corresponds to the time instance such that:

$$t_Q = \underset{t \in \boldsymbol{t}}{\arg\min} \left(\left| t - 2t_{\text{opt}} \right| \right) \tag{2}$$

The assumption behind the definition of t_Q is that the non-LoS delay is expected to be less than twice the direct transmission time (as exceeding the threshold would necessitate the use of a large test site, which is not considered here). Having that in mind, $\boldsymbol{P}_c$ analysis is confined within the reasonably narrow region (limited by t_Q) that is expected to contain both LoS responses (averaged across all $\boldsymbol{\theta}$ angles) and their combined first multi-path interferences. The time-instances $\boldsymbol{t}_\delta = \{t_{\delta.1}, t_{\delta.2}, \ldots\}$ that correspond to local maxima of the $\boldsymbol{P}_c$ vector are then identified and the expected delay resulting from multi-path propagation $t_{\max}$ is calculated as the first time-instance for which the gap between consecutive local maxima is greater than the average of $\boldsymbol{t}_\delta$.

The last step of the procedure involves the generation of a series of I (here, $I = 5$ is selected) low-pass finite impulse response filters (separately for each θ_a angle; based on the least-square approach) w.r.t. the constraints imposed by the identified LoS-to-non-LoS delays. The order of the filters is set to K/O, where $K = K_{\min} \cdot B \cdot M_F$ (with B being expressed in GHz) and $O = K/M_F$. The remaining parameters, i.e., $K_{\min} = 201$ and $M_F = 3$ represent the number of frequency points that ensure sufficient accuracy/cost balance (where cost is understood as the measurement time) and the factor that controls the maximum number of points allowed for synthesis of the prototype filters [13]. Note that each kernel is constructed w.r.t. the target time-domain response and then applied to the frequency-domain characteristics.

Let $\boldsymbol{\tau} = [\tau_1 \ \ldots \ \tau_{N1}]^T = ([t_1 \ \ldots \ t_{N1}]^T)/t_{N/2}$ and $\boldsymbol{\tau}_{s.a} = [\tau_{s.a.1} \ \ldots \ \tau_{s.a.I}]^T$ be the normalized time-sweep and a vector of I points bounded by $\tau_{s.a.1} = \tau_{0.a} - \rho_a \cdot \tau_{1.a}$ and $\tau_{s.a.I} = \tau_{0.a} + \rho_a \cdot \tau_{1.a}$, where $\tau_{0.a} = t_{0.a}^*/t_{N/2}$ and $\tau_{1.a} = w_0/t_{N/2}$ represent the center of the filter (extracted from the $\boldsymbol{t}_0$ vector) located with respect to the maximum of power response and the filter width. The upper limit that defines the feasible multiplication factor ρ_a for $\tau_{1.a}$ is given as:

$$\rho_a = \left\lfloor \frac{t_{\max}}{t_{N/2}\tau_{1.a}} - 1 \right\rfloor - 1 \tag{3}$$

The symbol $\lfloor \cdot \rfloor$ in (3) represents rounding down to the nearest integer. The ideal response of ith ($i = 1, \ldots, I$) low-pass filter is specified as $\boldsymbol{P}_{\text{ref}}(\boldsymbol{\tau}_{\text{ref}}) = [1 \ 1 \ 0 \ 0]^T$ with $\boldsymbol{\tau}_{\text{ref}} = [0, \ \tau_{s.a.i} + \tau_{1.a}, \ (1 + \tau_{2.a}) \cdot (\tau_{s.a.i} + \tau_{1.a}), t_{N/2}]$. The transition zone $\tau_{2.a}$ is given as:

$$\tau_{2.a} = \left| \frac{t_{N/2}}{\tau_{s.a.I} + \tau_{1.a}} - 1 \right| \tag{4}$$

Upon identification (which is realized using the *firls* function embedded in MATLAB), the ith kernel $\boldsymbol{R}_{\kappa.i}(\boldsymbol{\omega}, \theta_a)$ is applied to modify $\boldsymbol{R}(\boldsymbol{\omega}, \theta_a)$ using the zero-phase digital filtering (implemented as a part of MATLAB *filtfilt* routine) to generate the corrected $\boldsymbol{R}_{\gamma.i}(\boldsymbol{\omega}, \theta_a)$ response [16], [17]. Finally, the refined far-field performance of the AUT is obtained as follows:

$$\boldsymbol{R}_\gamma(\boldsymbol{\omega}, \theta_a) = \frac{1}{M} \sum_{i=1}^{I} \boldsymbol{R}_{\gamma.i}(\boldsymbol{\omega}, \theta_a) \tag{5}$$

It should be emphasized that $\boldsymbol{R}_\gamma(\boldsymbol{\omega}, \theta_a)$ represents the corrected frequency sweep w.r.t. θ_a angle. Upon execution of the refinement for all $\boldsymbol{\theta}$ angles, the final response—which corresponds the post-processed AUT radiation pattern obtained from non-anechoic measurements—is obtained from $\boldsymbol{R}_c(\boldsymbol{\omega}, \boldsymbol{\theta})$ as:

$$\boldsymbol{R}_c(f_0,\boldsymbol{\theta}) = \left[R_c(f_0,\theta_1)\ \ldots\ R_c(f_0,\theta_A)\right]^T \quad (6)$$

The above-discussed correction procedure can be summarized as follows (see Fig. 1 for visualization):

1. Set f_0, obtain $\boldsymbol{R}(\boldsymbol{\omega}, \boldsymbol{\theta})$;
2. Calculate Line-of-Sight to non-LoS delay based on a holistic, automatic analysis of $\boldsymbol{P}(\boldsymbol{t}, \boldsymbol{\theta})$;
3. Extract $\boldsymbol{R}_{\gamma,i}(\boldsymbol{\omega}, \theta_a)$ kernels, obtain $\boldsymbol{R}_c(\boldsymbol{\omega}, \boldsymbol{\theta})$ through filtering, and extract the $\boldsymbol{R}_c(f_0, \boldsymbol{\theta})$ response.

Note that the automatic analysis of $\boldsymbol{P}(\boldsymbol{t},\boldsymbol{\theta})$ is crucial for the identification of filters w.r.t. the Line-of-Sight signal (as a function of θ_a) while suppressing the interference-related noise. It should be emphasized that the analysis pertinent to the identification of filter kernels and correction of frequency responses is performed without the inference of the user. From this perspective, it is much more useful for day-to-day measurements compared to state-of-the-art post-processing routines.

III. Correction Results

The correction performance of the proposed framework has been demonstrated using the geometrically small antipodal Vivaldi antenna of Fig. 2. The structure has been measured in a 5.5 × 4.5 × 3.1 (length × width × height) m^3 non-anechoic test-site of Fig. 3 at a set of f_0 = {3.5 5.5 7.5 9.5} GHz frequencies. For each experiment, the bandwidth and the number of frequency points around f_0 required for post-processing have been set to B = 1 GHz and K = 603 (cf. Section II) [13].

Figure 4 represents a family of far-field characteristics obtained at the considered test site at the given frequencies before and after correction. It should be noted that the obtained post-processing results have been compared against the measurements performed in an anechoic chamber. The accuracy of the responses, expressed in terms of the root-mean-square error (averaged over the considered frequency points; RMSE), has been improved from –13.6 dB for uncorrected to –22.3 dB for refined responses, which represents 8.7 dB change (cf. Table I for a summary of the correction performance). The obtained results indicate that, for the considered test case and test frequencies, the presented correction mechanism offers a substantial improvement in the extracted AUT performance compared to direct non-anechoic measurements. It should be emphasized that setup of the post-processing process was limited just to the determination of the bandwidth around f_0 (based on recommendations from [13]), whereas identification of the low-pass filter parameters was performed without input from the user.

The performance of the proposed correction method has been validated against the state-of-the-art algorithms from the literature. The considered benchmark methods are based on time-domain correction where the gating functions intervals are identified as a result of: (i) manual determination of the test-site dimensions (with rectangular window), as well as (ii) visual inspection of the RA-AUT response (with Hann window) [5], [6], [19]. For fair comparison, the setup of each technique (in terms of B and K) is the same as specified above. The measurement data and the test-site also remain unchanged. The results gathered in Table I indicate that the presented approach outperforms the existing methods in terms of correction performance. For the considered test case, the average root-mean-square errors that result from the use of (i) and (ii) amount to –19.6 dB and –20.5 dB, which is 2.7 dB and 1.8 dB worse compared to the far-field responses obtained using the presented framework.

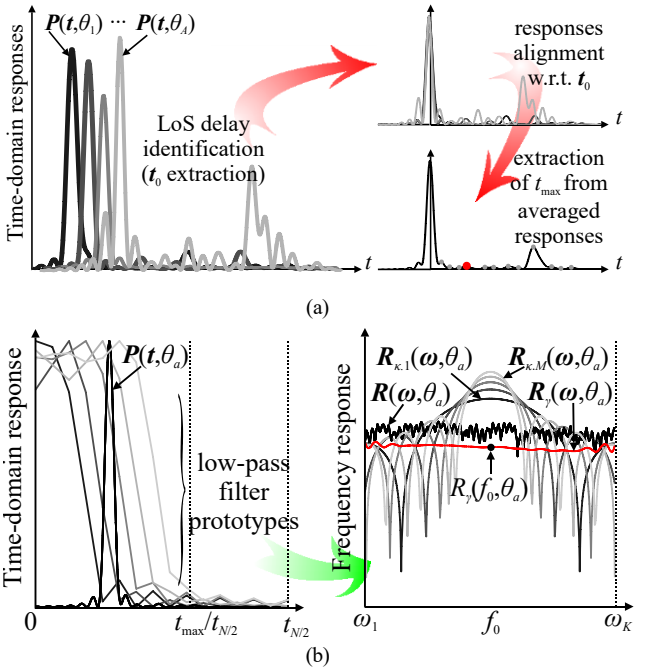

Fig. 1. Conceptual illustration of the proposed algorithm for correction of non-anechoic measurements: (a) extraction of LoS-to-non-LoS delay through automatic analysis of the power response (note that gray and red dots represent components of t_δ and t_{max} extracted from the $\boldsymbol{P}_c$ response) and (b) construction of the low-pass filter kernels followed by their application to the uncorrected response at θ_a angle.

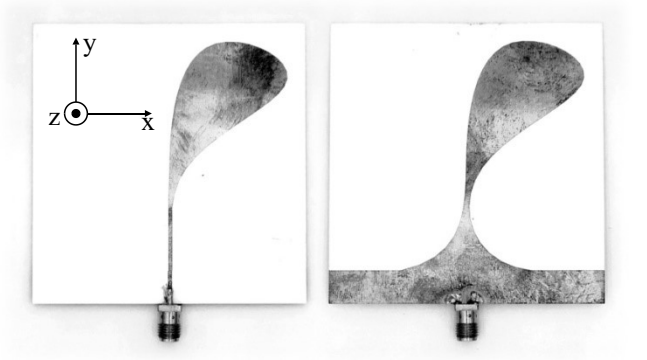

Fig. 2. Photographs (top and bottom) of a geometrically small antipodal Vivaldi antenna used for the experiments [13].

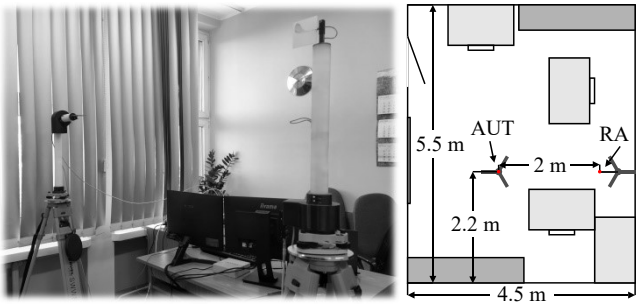

Fig. 3. A photograph (left) and the schematic view (right) of the non-anechoic test site considered for the experiments [18].

TABLE I. BENCHMARK OF THE PROPOSED METHOD

Method	Uncorrected	(i)	(ii)	This work
3.5 GHz (RMSE)	–10.9 dB	–17.7 dB	–20.2 dB	–21.1 dB
5.5 GHz (RMSE)	–13.2 dB	–15.4 dB	–17.8 dB	–21.1 dB
7.5 GHz (RMSE)	–13.7 dB	–22.6 dB	–21.1 dB	–23.2 dB
9.5 GHz (RMSE)	–16.6 dB	–22.6 dB	–22.9 dB	–23.6 dB

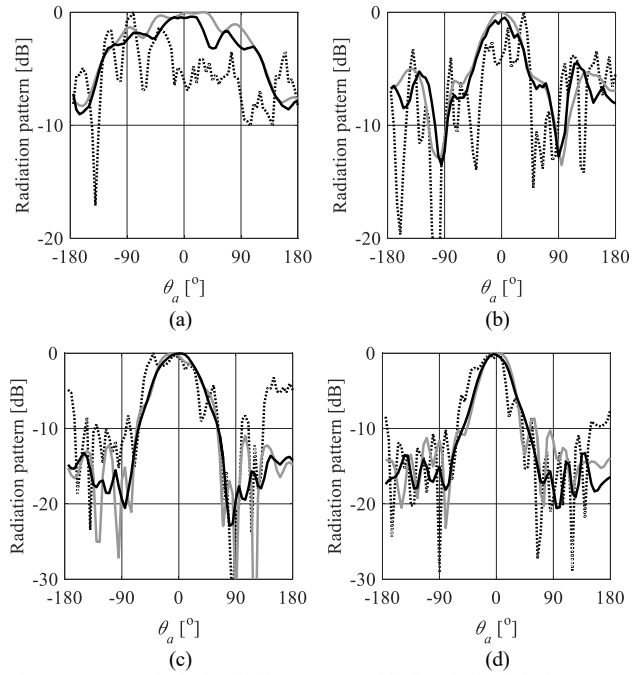

Fig. 4. Non-anechoic far-field responses (black) obtained before (···) and after (—) low-pass-filters-based correction vs. AC data (gray) at: (a) 3.5 GHz, (b) 5.5 GHz, (c) 7.5 GHz, and (d) 9.5 GHz frequencies.

IV. CONCLUSION

In this work, a framework for automatic correction of antenna measurements performed in non-anechoic environments has been proposed. The presented algorithm implements automatic analysis of the power impulse response in order to extract the LoS-to-non-LoS delays within the RA-AUT system as a function of angular position. The resulting delays are used for the identification of the low-pass filter prototypes that are then applied to modify the noisy frequency-domain responses of the AUT obtained in uncontrolled conditions. The method has been demonstrated through measurements of the geometrically small Vivaldi antenna in the office room that has not been tailored to far-field measurements. The obtained results indicate that, for the considered structure and frequencies, the average improvement of the responses due to post-processing amounts to around 9 dB. Furthermore, the approach has been favorably compared against the state-of-the-art methods from the literature.

Future work will focus on enhancing the method so as to enable automatic determination of the optimum bandwidth and the number of points around the frequency of interest. The development of techniques that combine various correction mechanisms in order to increase the amount of information on the propagation conditions will also be considered.

ACKNOWLEDGMENT

This work was supported in part by the National Science Center of Poland Grant 2021/43/B/ST7/01856, National Center for Research and Development Grant NOR/POLNOR /HAPADS/0049/2019-00, as well as Gdansk University of Technology (Excellence Initiative – Research University) Grant 16/2023/IDUB/IV.2/EUROPIUM.

REFERENCES

[1] L. Hemming, *Electromagnetic Anechoic Chambers: A fundamental Design and Specification Guide*, IEEE Press, Piscataway, 2002.

[2] M.S. Khan, *et al.*, "A compact CSRR-enabled UWB diversity antenna," *IEEE Ant. Wireless Prop. Lett.*, vol. 16, pp. 808-812, 2017.

[3] M.K. Megha and M. Jayakumar, "Circularly polarized stub-loaded annular ring patch antenna for 2×2 MIMO satellite application," *Measurement*, vol. 217, art no. 113044, 2023.

[4] A. Bekasiewicz and S. Koziel, "Structure and design optimisation of compact UWB slot antenna," *Electronics Lett.*, vol. 52, no. 9, pp. 681-682, 2016.

[5] S. Loredo, M.R. Pino, F. Las-Heras, and T.K. Sarkar, "Echo identification and cancellation techniques for antenna measurement in non-anechoic test sites," *IEEE Ant. Prop. Mag.*, vol. 46, no. 1, pp. 100-107, 2004.

[6] A. Soltane, G. Andrieu, E. Perrin, C. Decroze, and A. Reineix, "Antenna radiation pattern measurement in a reverberating enclosure using the time-gating technique," *IEEE Ant. Wireless Prop. Lett.*, vol. 19, no. 1, pp. 183-187, 2020.

[7] A.N. de Sao Jose, V. Deniau, U.C. Resende, and R. Adriano, "Improving antenna gain estimations in non-ideal test sites with auto-tunable filters," *Measurement*, vol. 159, art no. 107720, 2020.

[8] P. Piasecki and J. Strycharz, "Measurement of an omnidirectional antenna pattern in an anechoic chamber and an office room with and without time domain signal processing," *Signal Proc. Symp.*, pp. 1-4, Debe, Poland, 2015.

[9] Y. Su and S. Gong, "Reflection suppression through modal filtering for wideband antenna measurement in a non-absorbent environment," *Electronics*, vol. 11, no. 20, art. no. 3422, 2022.

[10] B. Fourestie, Z. Altman, J. Wiart, and A. Azoulay, "On the use of the matrix-pencil method to correlate measurements at different test sites," *IEEE Trans. Ant. Prop.*, vol, 47, no. 10, pp. 1569-1573, 1999.

[11] Z. Du, J.I. Moon, S.-S. Oh, J. Koh, and T.K. Sarkar, "Generation of free space radiation patterns from non-anechoic measurements using Chebyshev polynomials," *IEEE Trans. Ant. Prop.*, vol. 58, no. 8, pp. 2785-2790, 2010.

[12] J. Knapp, J. Kornprobst, and T.F. Eibert, "Equivalent source and pattern reconstruction from oversampled measurements in highlyreflective environments," *IET Microwaves, Ant. Prop.*, vol. 13 no. 13, pp. 2232-2241, 2019.

[13] A. Bekasiewicz, S. Koziel, and M. Czyz, "Time-gating method with automatic calibration for accurate measurements of electrically small antenna radiation patterns in non-anechoic environments," *Measurement*, vol. 208, art no. 112477, 2023.

[14] J. Koh, A. De, T.K. Sarkar, H. Moon, W. Zhao, and M. Salazar-Palma, "Free space radiation pattern reconstruction from non-anechoic measurements using an impulse response of the environment," *IEEE Trans. Ant. Prop.*, vol. 60, no. 2, pp. 821-831, 2012.

[15] S.M. Froes, P. Corral, M.S. Novo, M. Aljaro, and A.C.C. Lima, "Antenna radiation pattern measurement in a nonanechoic chamber," *IEEE Ant. Wireless Prop. Lett.*, vol. 18, no. 2, pp. 383-386, 2019.

[16] S.K. Mitra, *Digital Signal Processing*, 2nd ed., McGraw-Hill, 2001.

[17] M.X. Cohen, *Analyzing Neural Time Series Data: Theory and Practice*, MIT Press, 2014.

[18] J. Olencki, *et al.*, "A low-cost system for far-field non-anechoic measurements of antenna performance figures," IEEE Access, vol. 11, pp. 39165-39175, 2023.

[19] A.V. Oppenheim, R.W. Schafer, *Discrete-Time Signal Processing*, 3rd ed., Prentice Hall, 2009.